Research Article | Vol. 13, No. 1 / 1 Jan 2023 / Optical Materials Express 171
Optical Materials EXPRESS

Low coercivity magnetoplasmonic crystal based on a thin permalloy film for magnetic field sensing applications

Dmitry V. Murzin,[1,*] Aleksandr Yu. Frolov,[2] Karen A. Mamian,[2] Victor K. Belyaev,[1] Andrey A. Fedyanin,[2] and Valeria V. Rodionova[1]

[1]The Sophia Kovalevskaya North-West Mathematical Research Center, Immanuel Kant Baltic Federal University, Kaliningrad 236016, Russia
[2]Faculty of Physics, Lomonosov Moscow State University, Moscow 119991, Russia
[*]dvmurzin@yandex.ru

Abstract: This research is devoted to the fabrication of 5-nm thick permalloy film-based magnetoplasmonic crystal for magnetic field sensing applications. Optical and magneto-optical activity of the magnetoplasmonic crystal is studied with the means of numerical modeling and spectroscopy techniques. The studied sample achieves sensitivity to an external DC magnetic field of 7.5 mOe in the 5.1 Oe required modulation AC magnetic field. Obtained experimental and modeling results can be used for the fabrication of cheaper and more energy-efficient sensing elements for magnetoplasmonic crystal-based magnetic field sensors due to the reduction of required ferromagnetic material and modulation magnetic field.

1. Introduction

Demand for custom products in medicine, robotics, science, and mechanical engineering makes leaders of the world market supplant classic production techniques towards more technologically complex and competitive manufacturing. One of the modern trends to achieve that is the implementation of an industrial internet of things [1] - a digital platform combining multiple sensors, machine lines, supply chains, and operators into a network, collecting all the data and transforming it into the information about manufacturing efficiency and ways to improve it. Among all the sensors required for such a network, magnetic field sensors are of the main interest since they are used in most industrial, electronic, and automotive devices for signal registering [2], compensation of environmental noise [3], or manipulation control [4].

Depending on the task and operating environment, magnetic field sensors can be of various shapes, linear dimensions, and operating principles [5]. However, the most limiting factor for the implementation of a magnetic field sensor in a manufacturing process is its price. Expensive magnetic field sensors like SQUID or optically-pumped spin relaxation free magnetometers are suitable for specified tasks, like biomedical applications, magnetic field detection in outer space, or in other fields where the use of expensive and highly sensitive detectors is reasonable [6–8]. Relatively inexpensive and ubiquitous magnetic field sensors used in manufacturing are based on Hall, magnetoresistance, magnetoimpedance, and fluxgate effects. Such sensors can be easily implemented in most electronic devices but their linear dimensions reduction results in a subsequent sensitivity and limit of detection decrease.

Existing technologies for the production of such sensors are also suitable for the manufacture of the cost comparable, highly sensitive and local magnetic field sensors based on high magneto-optical activity in monocrystalline bismuth rare-earth iron-garnet films [9] or on magneto-optical effects enhanced with the use of surface plasmon polaritons (SPPs) excitation [10,11]. SPPs are TM electromagnetic waves of light and free electrons collective oscillations at the dielectric/metal

#478112 https://doi.org/10.1364/OME.478112
Journal © 2023 Received 20 Oct 2022; revised 18 Nov 2022; accepted 21 Nov 2022; published 15 Dec 2022

Optical Materials EXPRESS

interface [12]. As evanescent waves, SPPs propagate along the dielectric/metal boundary and decay into both metal and dielectric layers. SPPs enhance electromagnetic field inside the metal layer resulting in the enhanced magneto-optical activity because magneto-optical effects are proportional to the electromagnetic field inside material [13].

Excitation of SPPs at the dielectric/metal interface is a result of phase-matching conditions fulfillment that is achieved with several experimental schemes: Kretschmann or Otto geometries [14,15], excitation with SNOM probe or diffraction on surface features [16–18]. Due to the developed infrastructure for nanostructured materials fabrication, the most convenient regime of the SPPs excitation is the use of diffraction gratings made of combined noble and ferromagnetic metals, called magnetoplasmonic crystals (MPlCs) [13]. In MPlCs, diffracted light components coinciding with the SPP's wavevector are coupled to surface plasmons leading to the compliance of phase-matching conditions. Wavevector conversation from light to SPPs appears as a sharp dip in the reflected or transmitted light spectra, called Wood's anomaly. It is related to the light diffraction and SPPs excitation in the wavelength region defined by the angle of light incidence, structure parameters and refraction indexes of MPlC layers. Consequently, in the same wavelength region, magneto-optical effects are resonantly enhanced [19–23].

MPlCs for magnetic field sensing can be opaque [24,25] or transparent [26,27], depending on the observable magneto-optical effect. Recently, a new approach for magnetic field detection with the use of MPlCs was presented. It is based on the detection of the SPPs enhanced transverse Kerr effect (TKE) of a 100 nm thick Fe film-based MPlC exposed to an external required modulation AC magnetic field. Measuring the AC field dependence in the presence of any DC magnetic field, it is possible to measure the magnitude of the applied DC field with the sensitivity of 10^{-6} Oe at a local area of 1 mm^2 in the modulation AC field of 14.6 Oe [28]. To minimize energy consumption and price of the device, magnetically soft 100 and 130 nm thick permalloy (Py) films were used reducing the AC field magnitude to 7.3 Oe [25]. This value can be decreased even more with the use of thin Py layers without significant losses in the functionality of the MPlC-based magnetic field sensor, thus, allowing to fabricate more energy efficient sensing elements.

In this work, we propose a 5-nm thick Py film-based MPlC with the low coercive force for the reduction of the AC modulating field required for the magnetic field measurements. Before the fabrication of the MPlC, its optical and magneto-optical properties were modeled by the finite-difference time-domain (FDTD) method to define suitable geometrical parameters of the MPlC for further sensing applications. Experimentally measured reflectivity and TKE spectra of the fabricated sample are compared with the modeled dependencies. Magnetic properties of the fabricated sample were measured with the Kerr and vibrating sample magnetometry to estimate local and volume values of the sample's coercive field. It is shown that the MPlC has twice lower coercive field and measurable field region comparable to previously published results.

2. Materials and methods

Proposed MPlC had a trilayer structure of Ag (250 nm)/$Ni_{80}Fe_{20}$ (5 nm)/Si_3N_4 (10 nm) layers applied on the surface of a one-dimensional quasi-sinusoidal diffraction grating with the period of 320 nm and diffraction stripes height of 20 nm. The optical and magneto-optical activity of the magnetoplasmonic crystal were modeled with the use of the Lumerical FDTD software package. In simulations the sample was illuminated by a plane wave propagating at a fixed angle of 68°, corresponding to the maximum TKE value for such MPlCs [20]. When an external magnetic field is applied to the sample, the dielectric permittivity tensor ε of $Ni_{80}Fe_{20}$ becomes anisotropic. Its non-zero off-diagonal elements ε_{xy} and ε_{yx} are equal to $\pm ig$, where g is the gyration constant taken from experimental data in Ref. [29]. To model the TKE, reflection spectra were simulated

Optical Materials EXPRESS

in two opposite directions of the magnetic field. The TKE value was calculated with the formula:

$$TKE(\lambda) = 2\frac{R(+H) - R(-H)}{R(+H) + R(-H)}, \tag{1}$$

where $R(\pm H)$ are reflectance coefficients at the opposite magnetization directions

The DC magnetron sputtering method was used to prepare the MPlC with the corresponding layers' thickness, period, and stripes height on top of the polymer substrate. Sputtering was performed with the ORION-8-UHV magnetron sputtering setup at room temperature in the atmosphere of argon with a flow of 6 ppm. The source power was 75 W and the pressure in a chamber was 3 mTorr. Reference sample with the same composition based on the flat Si (100) substrate was made in the same sputtering cycle. The morphology of the prepared MPlC was studied with the atomic force microscope (AFM) NTEGRA AURA in a semi-contact mode. Magnetic properties of the MPlC in the external magnetic field directed along the easy magnetization axis (EMA) were studied with the NanoMOKE III magneto-optical Kerr magnetometer (MOKE) in the longitudinal Kerr effect geometry and with the vibrating sample magnetometer (VSM) LakeShore 7400. Additionally, a vector magnetometry hysteresis loop along EMA in the transverse geometry of the applied field, corresponding to the hard magnetization axis (HMA), was obtained with the Evico Magnetics magneto-optical Kerr microscope & magnetometer. MPlC reflectivity and TKE spectral dependencies in the visible wavelength region were studied with the optical setup consisting of a halogen lamp, two Glan–Taylor prisms as p-polarizer for the SPPs excitation and analyzer, a system of collimation lenses, Helmholtz coils, an optomechanical chopper, a SR830 Lock-in amplifier and a photomultiplier tube as a detector. The angle of the light incidence was equal to 68° corresponding to the -1^{st} diffraction order in accordance with the diffraction grating formula. For optical measurements, the light beam was modulated with the optomechanical chopper at the frequency of 298 Hz and for the TKE studies, the sample was exposed to the AC saturating modulation magnetic field with the magnitude of 250 Oe and frequency of 68 Hz. To calculate the TKE value from the experimentally obtained spectra, the following equation was used:

$$TKE(\lambda) = \frac{R(+H) - R(-H)}{R_0}, \tag{2}$$

where R_0 is the reflectivity amplitude in absence of the magnetic field. To compare the proposed MPlC with previously studied samples [25,28,30], the dependence of the TKE on the AC modulation magnetic field magnitude H_{AC} was studied and signal-to-noise ratio (SNR_{AC}) was calculated as:

$$SNR_{AC} = \frac{R(+H) - R(-H)}{\sigma}, \tag{3}$$

where σ is a noise standard deviation measured in the saturation magnetic field for $N = 500$ acquisition points.

3. Results and discussion

The studied MPlC shown in Fig. 1(a) has a geometry-driven anisotropy of magnetic properties formed by the diffraction grating [31]. The easy magnetization axis (EMA) of the MPlC is directed along the stripes and the hard magnetization axis (HMA) is perpendicular to them. Because application of a magnetic field along the diffraction stripes corresponds to the case of the SPPs enhanced TKE, hysteresis loops along the EMA are of particular interest [19]. The MPlC remagnetization along the EMA is mostly driven by the domain wall movement leading to high squareness ratio of the hysteresis loop independent of the measurement method. This can be seen from the measured hysteresis loops shown in Fig. 1(b).

Optical Materials EXPRESS

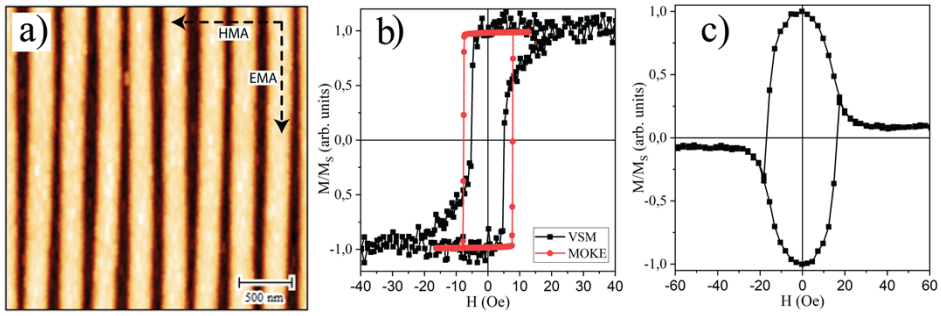

Fig. 1. (a) Atomic force microscopy image of the magnetoplasmonic crystal. Arrows correspond to the easy (EMA) and hard (HMA) magnetization axes of the sample. (b) Hysteresis loops of the magnetoplasmonic measured along the EMA with the magneto-optical Kerr magnetometer (MOKE, red line with circles) and vibrating sample magnetometer (VSM, black line with rectangles). (c) The vector magnetometry hysteresis loop along EMA in the magnetic field applied along HMA.

The shape difference between loops is due to the MOKE and VSM methods' features. The MOKE is sensitive to the magnetic moment in a small volume at the MPlC center area and the VSM is sensitive to the magnetic moment of the whole sample including its edge defects. The coercive field H_C of the MPlC was 7.7 Oe and 5.2 Oe according to the MOKE and VSM magnetometry, respectively. A higher coercive field in the case of MOKE magnetometry is a result of the MPlC center magnetization switching in larger magnetic fields, which can be observed for similar structures [31].

To verify the absence of magnetic interactions between MPlC stripes and the discontinuity of the sputtered Py layer, we obtained the vector magnetometry hysteresis loop, shown in Fig. 1(c). The measured magnetic moment is proportional to the projection of the magnetic moment of the sample along the EMA while the external magnetic field is aligned along the HMA. In absence of the applied magnetic field, most magnetization vectors are aligned along the EMA that is in accordance with the MOKE and VSM results. With the increase of the applied magnetic field, magnetization vectors start following the external magnetic field until the magnetization along the EMA reaches almost zero. Absence of any additional phases in this process is a result of the coherent rotation of magnetization vectors indicating no magnetic interactions between structure parts and continuity of the sputtered Py layer [32]. Kerr rotation in high magnetic fields and the magnetic moment along the EMA, respectively, does not vanish due to a small misalignment of the external magnetic field and the HMA direction, which can be explained by the domain splitting phase in the remagnetization process [33].

Results of the reflectivity and TKE preliminary modeling for the fabricated MPlC are shown in Fig. 2(a, b). Modeled reflectivity spectra (Fig. 2(a), dashed black line) possess an asymmetric Fano-shape profile consisting of the peak and following sharp dip. The peak is related to the diffracted light propagation along the MPlC surface, called the Rayleigh anomaly, and the dip is related to the fulfillment of the phase-matching of the incident light and surface plasmon polaritons, called the Wood anomaly. Spectral positions of the Rayleigh and Wood anomalies were λ=616 nm and λ=631 nm, respectively. Shape, width, and amplitude of the Wood anomaly depend on the sample's profile parameters and composition [34], as well as on the angle of light incidence [16]. Spectral position of the Rayleigh anomaly is defined by the diffraction grating formula and the Wood anomaly is associated with the excitation of the SPPs in a narrow spectral range [35]. Both resonant features depend on the MPlC composition and can undergo a spectral shift depending on the sample's functional layers' thicknesses [36] and profile parameters [22,37–39]. In the same wavelength region of the TKE spectrum (Fig. 2(b), red dashed line),

Optical Materials EXPRESS

a Fano-shape resonance, being a result of the SPP wave vector modulation by the external magnetic field, was observed. The TKE is significantly enhanced up to 1.2% at the resonant wavelength $\lambda = 640$ nm with respect to the reference sample based on a flat Si substrate with the same composition as the studied MPlC. Both optical and magneto-optical resonant features in preliminary modeled spectra were detected in the experimentally obtained reflectivity (open black circles) and TKE (red open circles) spectra shown in Fig. 2(a, b). The spectral position of the Rayleigh anomaly in the reflectivity spectra was the same as for the modeled result, but the spectral position of the Wood anomaly was shifted to λ=640 nm. Because the TKE resonance's spectral position is defined by the Wood anomaly, it was also shifted to the higher wavelength region in comparison to the modeled result. Amplitudes of both resonant features were also slightly different for modeled and experimental spectra due to the difference between materials' permittivity in the modeled and fabricated MPlC or due to a slightly different thicknesses of MPlC's functional layers formed by the magnetron sputtering method. A better resemblance between experimental results and numerical simulations of the reflectivity and TKE spectra was obtained with the modified model where the thicknesses of the Py and silica nitride layers in the model were changed to 4 nm and 12 nm, respectively. Results of the simulated reflectivity (solid black line) and TKE (red solid line) spectral dependences are shown in Fig. 2(a) and Fig. 2(b), respectively. In such a model, spectral position and width of the reflectivity minima coincided with the experimentally obtained dependence while the Fano-shape resonance in the TKE spectra was 5 nm shifted in the region of smaller wavelengths with respect to the experimentally obtained data. It should be noted that the simulated spectral dependence of TKE and the maximal TKE value are similar for both simulation models. These spectral dependence's shape and values are in good agreement with experimental TKE spectra. Therefore, a slight change of the Py layer thickness on 1 or 2 nm during the MPlC fabrication process does not significantly modify TKE spectral dependence, maximal TKE value and MPlC performance for sensing applications. However, further deviation of the layers' thicknesses in the simulation model can significantly change the reflectance spectrum and TKE values in the MPlC. To verify the SPPs excitation, near-field simulations were performed for the modified MPlC model. Figure 2(c) demonstrates $|\mathbf{E}|^2$ distribution at λ=640 nm corresponding to the simulated TKE maximum (solid line in Fig. 2(b)). Electric field is strongly enhanced near the MPlC interface due to the SPP excitation. It provides higher sensitivity of the MPlC to the external magnetic field in comparison with nonstructured films that do not support SPP [40].

The working principle of the proposed sensing element is based on the measurement of a magnetic field-dependent magneto-optical signal change caused by the addition of a DC magnetic field to the MPlC exposed to the constantly applied AC modulation field with the H_{MOD} magnitude [28]. This type of dependences is measured at a resonant wavelength resulting in the magneto-optical activity enhancement [40] that can be expressed in terms of the *SNR* shown in Fig. 3.

The measurable field region and ΔSNR_{AC} is proportional to the detectable signal. Values were calculated according to the *FWHM* of the dependence first derivative. The center of the dependence's slope, calculated from its first derivative maximum, denotes the working point of the sensing element, and the required value of the modulation magnetic field H_{MOD} that was 5.1 Oe for the proposed sample. The sensitivity of the assembled setup to the applied DC magnetic field was limited by the signal deviation from the H_{MOD}, equal to 7.5 mOe.

Optical Materials EXPRESS

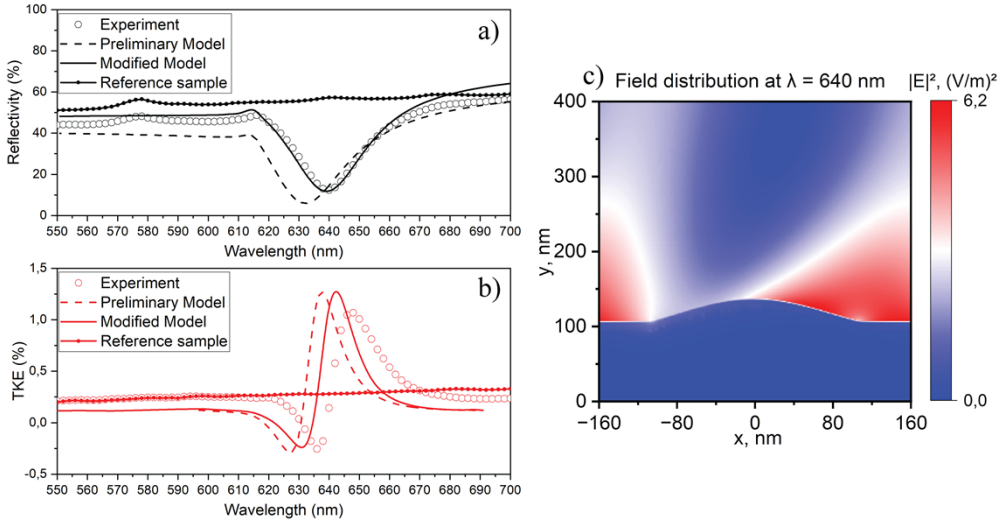

Fig. 2. Experimental results (blank circles), preliminary model (dash line), and modified model (solid line) of MPlC (a) reflectivity and (b) TKE spectra. Solid lines with circles correspond to the reference sample spectral dependencies of reflectivity (black) and TKE (red). (c) Simulation of the $|E|^2$ near-field distribution at the metal/dielectric interface of the MPlC.

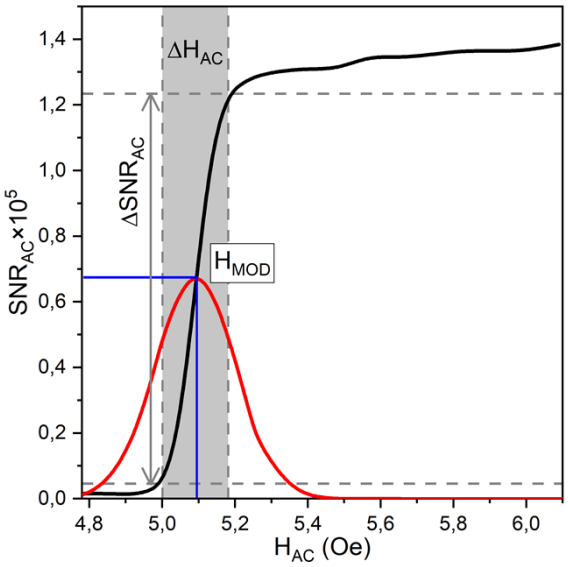

Fig. 3. SNR_{AC} dependence (black line) where H_{MOD} is the center of the dependence slope and ΔH is a measurable field region. H_{MOD} and ΔH were calculated according to the maximum and *FWHM* of the SNR_{AC} first derivative (red solid line), respectively.

Optical Materials EXPRESS

4. Conclusions

To conclude, magnetic, optical, and magneto-optical properties of the one-dimensional magneto-plasmonic crystal based on a thin permalloy film were experimentally and numerically studied. Numerical simulations of the reflectivity and the transversal Kerr effect spectra are in good accordance with experimental results and provide the geometrical parameters for the fabrication of magnetoplasmonic crystals with different compositions for sensing applications. Demonstrated parameters H_{MOD}, ΔH, and ΔSNR_{AC} allow the use of the fabricated sample for magnetic field detection without losses in functional properties. The use of a magnetically soft thin permalloy layer led to the two-fold reduction of ΔH_{MOD} and value of the required modulation field as well as one order decrease of ΔSNR_{AC} in comparison with previously shown data. Reduction of the modulation field value allows one to use smaller and less energy consuming electromagnets to produce cheaper, more energy efficient and size-minimized magnetic field sensors based on magnetoplasmonic crystals.

Funding. Ministry of Science and Higher Education of the Russian Federation (075-02-2022-872).

Acknowledgments. Authors thank Andrey A. Grunin from the Lomonosov Moscow State University Faculty of Physics for valuable and constructive comments.

Disclosures. The authors declare no conflicts of interest.

Data availability. Data underlying the results presented in this paper are not publicly available at this time but may be obtained from the authors upon reasonable request.

References

1. E. Sisinni, A. Saifullah, S. Han, U. Jennehag, and M. Gidlund, "Industrial internet of things: challenges, opportunities, and directions," IEEE Trans. Ind. Inf. **14**(11), 4724–4734 (2018).
2. L. Jogschies, D. Klaas, R. Kruppe, J. Rittinger, P. Taptimthong, A. Wienecke, L. Rissing, and M. Wurz, "Recent developments of magnetoresistive sensors for industrial applications," Sensors **15**(11), 28665–28689 (2015).
3. Y.-L. Song, H.-Y. Lin, S. Manikandan, and L.-M. Chang, "A magnetic field canceling system design for diminishing electromagnetic interference to avoid environmental hazard," Int. J. Environ. Res. Public Health **19**(6), 3664 (2022).
4. T. Reininger, F. Welker, and M. von Zeppelin, "Sensors in position control applications for industrial automation," Sens. Actuators, A **129**(1-2), 270–274 (2006).
5. J. E. Lenz, "A review of magnetic sensors," Proc. IEEE **78**(6), 973–989 (1990).
6. R. Stolz, M. Schmelz, V. Zakosarenko, C. P. Foley, K. Tanabe, X. Xie, and R. Fagaly, "Superconducting sensors and methods in geophysical applications," Supercond. Sci. Technol. **34**(3), 033001 (2021).
7. J. S. Bennett, B. E. Vyhnalek, H. Greenall, E. M. Bridge, F. Gotardo, S. Forstner, G. I. Harris, F. A. Miranda, and W. P. Bowen, "Precision Magnetometers for Aerospace Applications: A Review," Sensors **21**(16), 5568 (2021).
8. D. Murzin, D. J. Mapps, K. Levada, V. Belyaev, A. Omelyanchik, L. Panina, and V. Rodionova, "Ultrasensitive Magnetic Field Sensors for Biomedical Applications," Sensors **20**(6), 1569 (2020).
9. A. E. Rogachev, P. M. Vetoshko, N. A. Gusev, M. A. Kozhaev, A. R. Prokopov, V. V. Popov, D. V. Dodonov, A. G. Shumilov, A. N. Shaposhnikov, V. N. Berzhansky, A. K. Zvezdin, and V. I. Belotelov, "Vector magneto-optical sensor based on transparent magnetic films with cubic crystallographic symmetry," Appl. Phys. Lett. **109**(16), 162403 (2016).
10. C. Rizal, M. G. Manera, D. O. Ignatyeva, J. R. Mejía-Salazar, R. Rella, V. I. Belotelov, F. Pineider, and N. Maccaferri, "Magnetophotonics for sensing and magnetometry toward industrial applications," J. Appl. Phys. **130**(23), 230901 (2021).
11. N. Maccaferri, I. Zubritskaya, I. Razdolski, I.-A. Chioar, V. Belotelov, V. Kapaklis, P. M. Oppeneer, and A. Dmitriev, "Nanoscale magnetophotonics," J. Appl. Phys. **127**(8), 080903 (2020).
12. S. A. Maier, *Plasmonics: Fundamentals and Applications* (Springer US, 2007).
13. G. Armelles, A. Cebollada, A. García-Martín, and M. U. González, "Magnetoplasmonics: combining magnetic and plasmonic functionalities," Adv. Opt. Mater. **1**(1), 10–35 (2013).
14. N. Bonod, R. Reinisch, E. Popov, and M. Nevière, "Optimization of surface-plasmon-enhanced magneto-optical effects," J. Opt. Soc. Am. B **21**(4), 791–797 (2004).
15. F. Ramos-Mendieta, J. A. Hernández-López, and M. Palomino-Ovando, "Transverse magnetic surface plasmons and complete absorption supported by doped graphene in Otto configuration," AIP Adv. **4**(6), 067125 (2014).
16. H. Raether, *Surface Plasmons on Smooth and Rough Surfaces and on Gratings*, Springer Tracts in Modern Physics (Springer Berlin Heidelberg, 1988), 111.
17. A. L. Chekhov, P. N. Naydenov, A. I. Stognij, and T. V. Murzina, "Optical effects in magnetoplasmonic crystals with buried gold grating," in *Frontiers in Optics 2017* (OSA, 2017), **4**(6), p. JW3A.101.

Optical Materials EXPRESS

18. A. Y. Frolov, N. Verellen, V. V. Moshchalkov, and A. A. Fedyanin, "Subwavelength probing of surface plasmons in magnetoplasmonic crystals," J. Phys.: Conf. Ser. **2015**(1), 012041 (2021).
19. V. I. Belotelov, I. A. Akimov, M. Pohl, V. A. Kotov, S. Kasture, A. S. Vengurlekar, A. V. Gopal, D. R. Yakovlev, A. K. Zvezdin, and M. Bayer, "Enhanced magneto-optical effects in magnetoplasmonic crystals," Nat. Nanotechnol. **6**(6), 370–376 (2011).
20. A. A. Grunin, A. G. Zhdanov, A. A. Ezhov, E. A. Ganshina, and A. A. Fedyanin, "Surface-plasmon-induced enhancement of magneto-optical Kerr effect in all-nickel subwavelength nanogratings," Appl. Phys. Lett. **97**(26), 261908 (2010).
21. N. Maccaferri, X. Inchausti, A. García-Martín, J. C. Cuevas, D. Tripathy, A. O. Adeyeye, and P. Vavassori, "Resonant enhancement of magneto-optical activity induced by surface plasmon polariton modes coupling in 2D magnetoplasmonic crystals," ACS Photonics **2**(12), 1769–1779 (2015).
22. M. A. Kiryanov, A. Y. Frolov, I. A. Novikov, P. A. Kipp, P. K. Nurgalieva, V. V. Popov, A. A. Ezhov, T. V. Dolgova, and A. A. Fedyanin, "Surface profile-tailored magneto-optics in magnetoplasmonic crystals," APL Photonics **7**(2), 026104 (2022).
23. A. V. Chetvertukhin, A. A. Grunin, T. V. Dolgova, M. Inoue, and A. A. Fedyanin, "Transversal magneto-optical Kerr effect in two-dimensional nickel magnetoplasmonic crystals," J. Appl. Phys. **113**(17), 17A942 (2013).
24. J. Qin, L. Deng, T. Kang, L. Nie, H. Feng, H. Wang, R. Yang, X. Liang, T. Tang, J. Shen, C. Li, H. Wang, Y. Luo, G. Armelles, and L. Bi, "Switching the optical chirality in magnetoplasmonic metasurfaces using applied magnetic fields," ACS Nano **14**(3), 2808–2816 (2020).
25. V. K. Belyaev, D. V. Murzin, N. N. Perova, A. A. Grunin, A. A. Fedyanin, and V. V. Rodionova, "Permalloy-based magnetoplasmonic crystals for sensor applications," J. Magn. Magn. Mater. **482**(August 2018), 292–295 (2019).
26. G. A. Knyazev, P. O. Kapralov, N. A. Gusev, A. N. Kalish, P. M. Vetoshko, S. A. Dagesyan, A. N. Shaposhnikov, A. R. Prokopov, V. N. Berzhansky, A. K. Zvezdin, and V. I. Belotelov, "Magnetoplasmonic crystals for highly sensitive magnetometry," ACS Photonics **5**(12), 4951–4959 (2018).
27. D. O. Ignatyeva, G. A. Knyazev, A. N. Kalish, A. I. Chernov, and V. I. Belotelov, "Vector magneto-optical magnetometer based on resonant all-dielectric gratings with highly anisotropic iron garnet films," J. Phys. D: Appl. Phys. **54**(29), 295001 (2021).
28. V. K. Belyaev, V. V. Rodionova, A. A. Grunin, M. Inoue, and A. A. Fedyanin, "Magnetic field sensor based on magnetoplasmonic crystal," Sci. Rep. **10**(1), 7133 (2020).
29. K. K. Tikuišis, L. Beran, P. Cejpek, K. Uhlířová, J. Hamrle, M. Vaňatka, M. Urbánek, and M. Veis, "Optical and magneto-optical properties of permalloy thin films in 0.7–6.4 eV photon energy range," Mater. Des. **114**, 31–39 (2017).
30. V. K. Belyaev, D. V. Murzin, A. G. Kozlov, A. A. Grunin, A. S. Samardak, A. V. Ognev, A. A. Fedyanin, M. Inoue, and V. V. Rodionova, "Engineering of optical, magneto-optical and magnetic properties of nickel-based one-dimensional magnetoplasmonic crystals," Jpn. J. Appl. Phys. **59**(SE), SEEA08 (2020).
31. V. K. Belyaev, A. G. Kozlov, A. V. Ognev, A. S. Samardak, and V. V. Rodionova, "Magnetic properties and geometry-driven magnetic anisotropy of magnetoplasmonic crystals," J. Magn. Magn. Mater. **480**(19), 150–153 (2019).
32. C. Daboo, J. A. C. Bland, R. J. Hicken, A. J. R. Ives, M. J. Baird, and M. J. Walker, "Vectorial magnetometry with the magneto-optic Kerr effect applied to Co/Cu/Co trilayer structures," Phys. Rev. B **47**(18), 11852–11859 (1993).
33. T. Kuschel, H. Bardenhagen, H. Wilkens, R. Schubert, J. Hamrle, J. Pištora, and J. Wollschläger, "Vectorial magnetometry using magnetooptic Kerr effect including first- and second-order contributions for thin ferromagnetic films," J. Phys. D: Appl. Phys. **44**(26), 265003 (2011).
34. C. Clavero, K. Yang, J. R. Skuza, and R. A. Lukaszew, "Magnetic-field modulation of surface plasmon polaritons on gratings," Opt. Lett. **35**(10), 1557 (2010).
35. A. A. Maradudin, I. Simonsen, J. Polanco, and R. M. Fitzgerald, "Rayleigh and Wood anomalies in the diffraction of light from a perfectly conducting reflection grating," J. Opt. **18**(2), 024004 (2016).
36. A. Hajebifard and P. Berini, "Fano resonances in plasmonic heptamer nano-hole arrays," Opt. Express **25**(16), 18566 (2017).
37. Z. Tang, R. Zhu, L. Chen, C. Zhang, Z. Zong, S. Tang, and Y. Du, "Tuning the magneto-optical Kerr effect by the nanograting cross section," Opt. Lett. **44**(7), 1666 (2019).
38. R. M. Rowan-Robinson, E. Melander, I.-A. Chioar, B. Caballero, A. García-Martín, E. T. Papaioannou, and V. Kapaklis, "Thickness dependent enhancement of the polar Kerr rotation in Co magnetoplasmonic nanostructures," AIP Adv. **9**(2), 025317 (2019).
39. R. Zhu, L. Chen, Z. Zong, Z. Tang, J. Qian, S. Tang, and Y. Du, "Tuning the shape of magneto-optical Kerr spectrum by changing the strip width in one-dimensional Ag-Co-Ag magnetoplasmonic nanogratings," Appl. Phys. Lett. **115**(7), 072405 (2019).
40. V. Belyaev, A. Grunin, A. Fedyanin, and V. Rodionova, "Magnetic and magneto-optical properties of magnetoplasmonic crystals," Solid State Phenom. **233-234**, 599–602 (2015).